Disturbed flow-activated p90RSK kinase accelerates atherosclerosis by inhibiting SENP2 function

Kyung-Sun Heo,[1] Nhat-Tu Le,[1] Hannah J. Cushman,[1] Carolyn J. Giancursio,[1] Eugene Chang,[1] Chang-Hoon Woo,[1] Mark A. Sullivan,[2] Jack Taunton,[3] Edward T.H. Yeh,[4] Keigi Fujiwara,[1] and Jun-ichi Abe[1]

[1]Aab Cardiovascular Research Institute and Department of Medicine, and [2]Department of Microbiology and Immunology, University of Rochester School of Medicine and Dentistry, Rochester, New York, USA. [3]Howard Hughes Medical Institute and Department of Cellular and Molecular Pharmacology, UCSF, San Francisco, California, USA. [4]Department of Cardiology, University of Texas MD Anderson Cancer Center, Texas Heart Institute, St. Luke's Episcopal Hospital, Houston, Texas, USA.

Disturbed blood flow (d-flow) causes endothelial cell (EC) dysfunction, leading to atherosclerotic plaque formation. We have previously shown that d-flow increases SUMOylation of p53 and ERK5 through downregulation of sentrin/SUMO-specific protease 2 (SENP2) function; however, it is not known how SENP2 itself is regulated by d-flow. Here, we determined that d-flow activated the serine/threonine kinase p90RSK, which subsequently phosphorylated threonine 368 (T368) of SENP2. T368 phosphorylation promoted nuclear export of SENP2, leading to downregulation of eNOS expression and upregulation of proinflammatory adhesion molecule expression and apoptosis. In an LDLR-deficient murine model of atherosclerosis, EC-specific overexpression of p90RSK increased EC dysfunction and lipid accumulation in the aorta compared with control animals; however, these pathologic changes were not observed in atherosclerotic mice overexpressing dominant negative p90RSK (DN-p90RSK). Moreover, depletion of SENP2 in these mice abolished the protective effect of DN-p90RSK overexpression. We propose that p90RSK-mediated SENP2-T368 phosphorylation is a master switch in d-flow–induced signaling, leading to EC dysfunction and atherosclerosis.

Introduction

Atherosclerosis is a focalized disease that develops preferentially in areas within large arteries that are exposed to disturbed blood flow (d-flow) (1, 2). Endothelial cells (ECs) are thought to sense and respond to different flow patterns. Indeed, d-flow, not steady laminar flow (s-flow), activates proinflammatory and proapoptotic genes in ECs, causing them to become dysfunctional and proatherogenic (3–5). SUMOylation plays an important role in regulating actin filament remodeling (6), migration (6, 7), inflammation (8), and apoptosis (3) that occur in ECs in response to flow stimulation (3, 4, 8). SUMOylation is one of the most dynamic posttranslational modifications, with its diverse repertoire of effects, such as the localization, transcriptional activity, and DNA binding of modified proteins (9–11). Previously, we found that d-flow induced SUMOylation of p53 (3) and ERK5 (12), leading to EC apoptosis and inflammation, respectively. Reduced expression of sentrin/SUMO-specific protease 2 (SENP2) increased p53 and ERK5 SUMOylation, hence accelerating EC dysfunction, inflammation, and consequently, atherosclerotic plaque formation in mice (11). Although these results might suggest SENP2 expression being downregulated by d-flow, we failed to detect such a change in ECs exposed to d-flow in vitro (11). Because p90RSK activation was associated with EC inflammation and apoptosis, we examined the role of p90RSK in regulating SUMOylation states of SENP2 substrates.

Conflict of interest: Jack Taunton is a cofounder of Principia Biopharma, which has licensed the p90RSK kinase inhibitor FMK-MEA.
Submitted: April 2, 2014; **Accepted:** January 6, 2015.
Reference information: *J Clin Invest*. 2015;125(3):1299–1310. doi:10.1172/JCI76453.

Results

p90RSK activation by d-flow induces EC apoptosis and inflammation. We first tested to determine whether d- or s-flow activated p90RSK using human umbilical vein ECs (HUVECs) and found that only d-flow significantly increased p90RSK phosphorylation (Figure 1, A and C) and expression in a time-dependent manner (Supplemental Figure 1; supplemental material available online with this article; doi:10.1172/JCI76453DS1), suggesting the unique response of p90RSK to d-flow. Of note, ERK5 activation was induced only by s-flow (Figure 1, B and C). d-flow–induced apoptosis (Figure 1, D and E) and proinflammatory adhesion molecule expression (Figure 1F) were inhibited in ECs transduced with adenovirus containing dominant negative p90RSK (K94A/K447A, Ad-DN-p90RSK), but not in those transduced with Ad-LacZ and WT-p90RSK. It is interesting to note that Ad-WT-p90RSK transduction by itself without d-flow stimulation significantly increased numbers of apoptotic cells and adhesion molecule expression, suggesting that a certain fraction of overexpressed p90RSK is constitutively activated (Figure 1, D–F). In addition, adhesion molecule expression induced by d-flow was further augmented by overexpression of WT-p90RSK (Figure 1F). Taken together, these data suggest that p90RSK plays a crucial role in regulating d-flow–induced EC apoptosis and inflammation.

Depletion of p90RSK abolishes d-flow–induced p53 and ERK5 SUMOylation. Because we have reported that d-flow SUMOylates p53 and ERK5 (11) and because both Ad-DN-p90RSK and a specific p90RSK kinase inhibitor, FMK-MEA, completely inhibit d-flow–induced p90RSK activation (refs. 13, 14, and Supplemental Figure 2B), p90RSK may play a role in p53 and ERK5 SUMOylation by

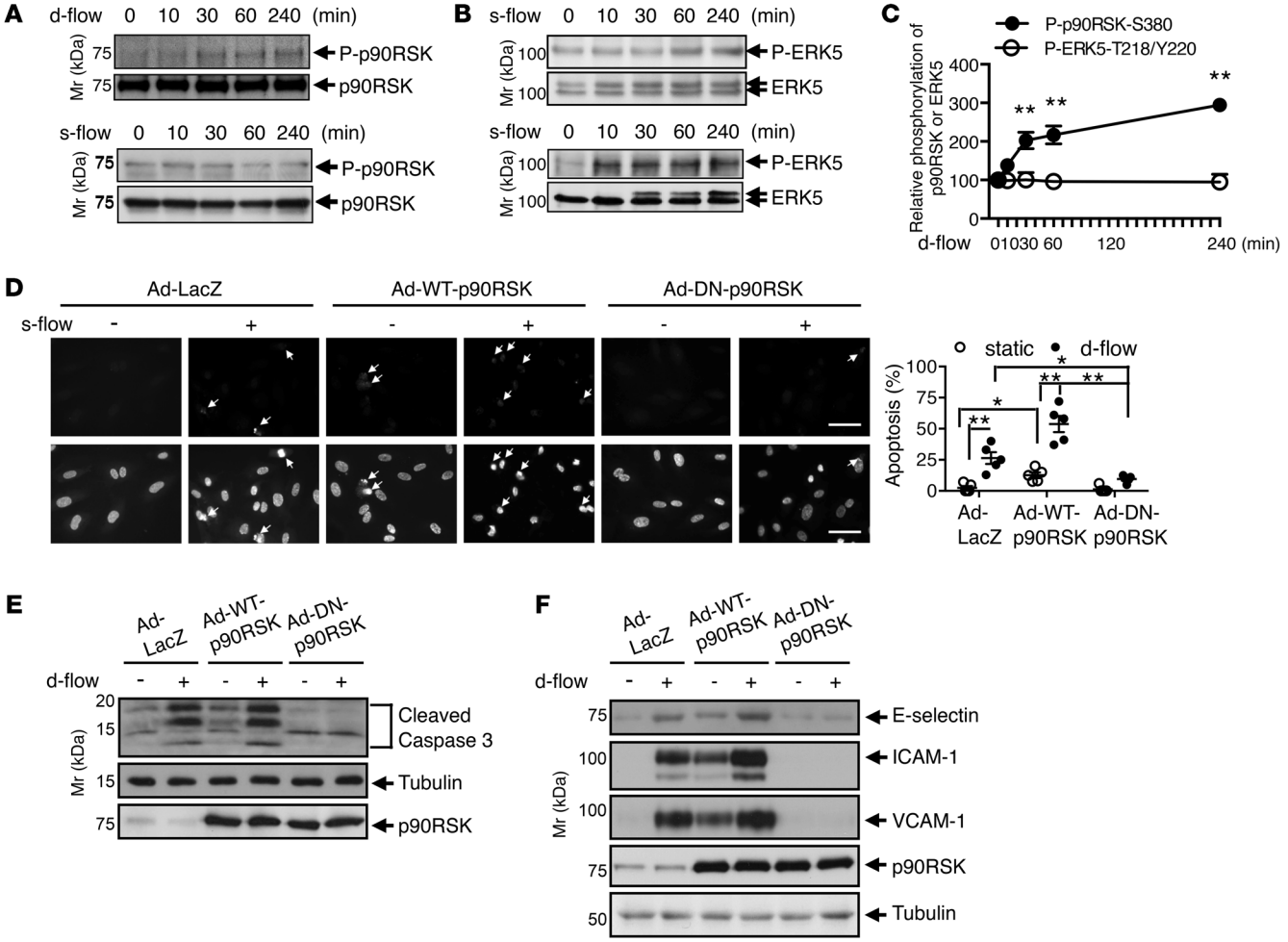

Figure 1. Role of p90RSK activation in d-flow–induced apoptosis and inflammation. (**A**–**C**) HUVECs were stimulated by d-flow (upper panel) or s-flow (lower panel) for indicated times, and p90RSK (**A**) and ERK5 (**B**) activation were examined by Western blotting using anti–phospho-p90RSK and anti–phospho-ERK5 (T218/Y220), respectively. (**C**) Quantification of d-flow–induced p90RSK and ERK5 activation is shown after normalization by total protein levels. Data represent mean ± SEM (0 minutes = 100, $n = 3$). (**D**) HUVECs were transduced with 50 MOI of Ad-LacZ, Ad-WT-p90RSK, or Ad-DN-p90RSK for 18 hours and then stimulated by d-flow or no flow for 36 hours, followed by TUNEL staining. Images were recorded as described in Methods after counterstaining with DAPI to visualize nuclei. Apoptotic nuclei are indicated by arrows (left panel). Quantification of apoptosis is shown as the percentage of TUNEL-positive cells (right panel). Data represent mean ± SEM, $n = 5$. Scale bars: 60 μm. (**E** and **F**) HUVECs were transduced with 50 MOI of Ad-LacZ, Ad-WT-p90RSK, or Ad-DN-p90RSK and then stimulated by d-flow for 24 hours. Expression of cleaved caspase-3 (**E**) or E-selectin, ICAM-1, VCAM-1, p90RSK, and tubulin (**F**) is shown. $^*P < 0.05$; $^{**}P < 0.01$, by 1-way ANOVA followed by Bonferroni's post hoc test.

d-flow. We deleted both p90RSK1 and -2 by siRNA and found that d-flow–induced p53 SUMOylation (Figure 2A) and the association of p53 with Bcl-2, which inhibits the antiapoptotic effect of Bcl-2 (ref. 3 and Supplemental Figure 2A), were completely inhibited. The complete inhibition of d-flow–induced p53 SUMOylation was also achieved by Ad-DN-p90RSK transduction and FMK-MEA (ref. 13 and Figure 2B). d-flow–induced ERK5 SUMOylation was also inhibited by Ad-DN-p90RSK transduction (Figure 2C). These data suggest that p90RSK kinase activity is involved in regulating SUMOylation of both p53 and ERK5 in ECs by d-flow.

p90RSK-mediated SENP2-T368 phosphorylation is regulated by SUMOylation of p53 and ERK5 and is critical for EC apoptosis and inflammation. Because we had earlier shown the involvement of both p90RSK kinase activity and SENP2 in d-flow–initiated signaling (11), we investigated whether p90RSK could directly phosphorylate SENP2. We found that 3 GST-tagged SENP2 fragments (1–130 aa, 131–300 aa, and 301–450 aa) were phosphorylated by recombinant p90RSK in vitro (Supplemental Figure 3A). We then subjected phosphorylated SENP2 to proteolytic digestion and liquid chromatography–tandem mass spectrometry (LC-MS/MS) and identified T35, S38, and T368 as SENP2 phosphorylation sites by p90RSK with a less than 0.05 error (Figure 3A). The predicted mass of each b or y fragment and the actual value are shown, with the y5 fragment containing the phosphorylated T368 having a predicted mass of 704.4 Da versus an actual value of 686.19 Da (Figure 3A). To study the effect of phosphorylation on downstream signaling, each phosphorylation site was mutated to alanine, expressed in ECs, and its effect on p90RSK-mediated p53 SUMOylation determined (Figure 3B). Inhibition of p53 SUMOylation induced by WT SENP2 (Figure 3B, lane 2) was completely lost in cells cotransfected with

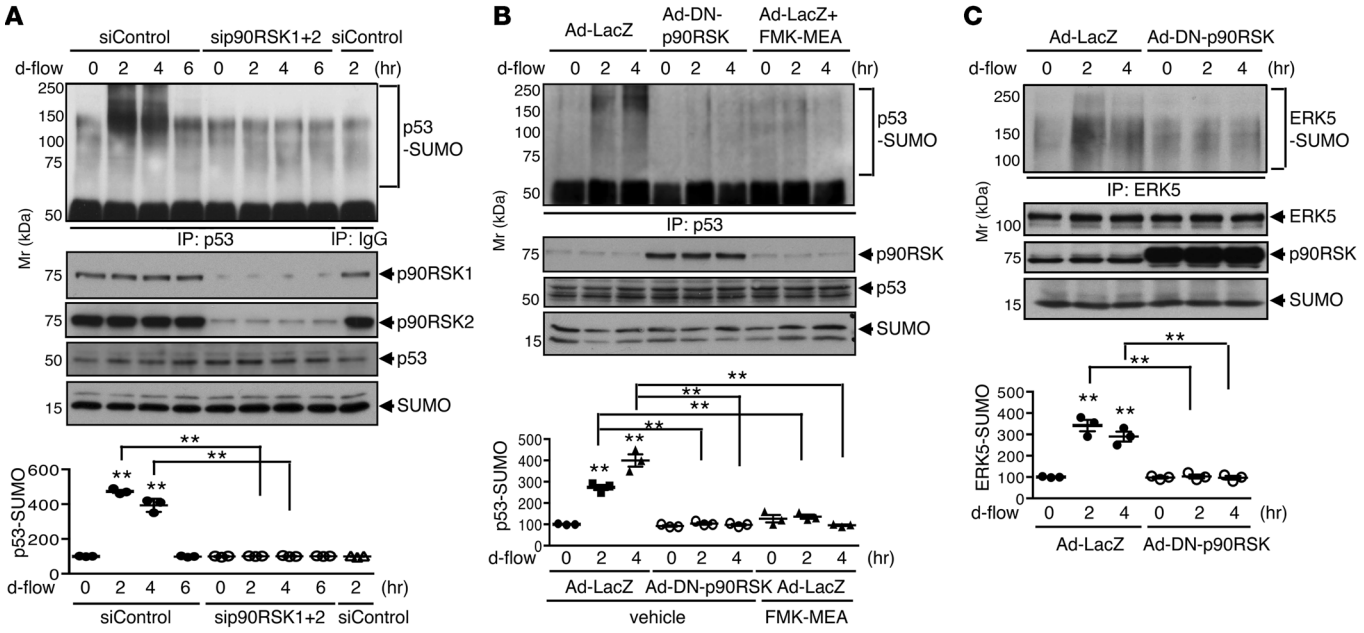

Figure 2. Depletion of p90RSK abolishes d-flow–induced p53 and ERK5 SUMOylation. (**A**) HUVECs were transfected with control siRNA or a mixture of siRNAs against p90RSK isoforms 1 and 2 followed by d-flow stimulation for indicated times. To detect p53 SUMOylation, anti-p53 or IgG was immunoprecipitated and immunoblotted with anti-SUMO. p90RSK1 and -2, p53, and SUMO expression were detected by Western blotting. Quantified data represent mean ± SEM (n = 3). (**B** and **C**) HUVECs were pretreated with either vehicle or FMK-MEA and then transduced with Ad-LacZ or Ad-DN-p90RSK followed by d-flow stimulation. SUMOylation of p53 (**B**) and ERK5 (**C**) were detected (upper panel). p90RSK, p53, ERK5, and SUMO expression were detected by Western blotting. Quantification of data represents mean ± SEM (lower panel, n = 3). $^{**}P < 0.01$, by 1-way ANOVA followed by Bonferroni's post hoc test. siControl, control siRNA.

p90RSK (Figure 3B, lane 3). Among the 3 SENP2 phosphorylation site mutants, the SENP2-T368A mutant (Figure 3B, lane 6), but not T35A and S38A mutants, was able to completely block this inhibitory effect (Figure 3, B and C).

Next, we investigated whether d-flow could increase SENP2-T368 phosphorylation using a synthetic human antibody against phospho–SENP2-T368 we generated by employing a phage display system. In order to establish the specificity of this antibody, we generated adenovirus vector containing mouse SENP2-WT or 1 of the 3 phosphorylation mutants (T35A, S38A, and T368A) and transduced ECs. By Western blotting, the phospho–SENP2-T368 antibody detected d-flow–induced SENP2 phosphorylation in ECs transduced by SENP2-WT, T35A, and T38A, but the SENP2-T368A mutant was not detected by this antibody (Figure 3D), indicating its T368 phospho-specificity. To confirm the SENP2 phosphorylation site by p90RSK, an in vitro kinase assay was performed, and we found that recombinant p90RSK phosphorylated immunoprecipitated SENP2, which was detected by the anti–phospho–SENP2-T368 antibody (Supplemental Figure 3B). We detected no band corresponding to total SENP2 or phospho–SENP2-T368 in nonimmune control IgG immunoprecipitates.

Although T368 is conserved in mouse and human, there are 2 aa differences within a sequence of 10 residues surrounding T368 between human (DLL*EL*TEDME) and mouse (DLF*EF*TEDME). Therefore, we also investigated whether p90RSK can phosphorylate human SENP2-T368. We cotransfected HUVECs with Flag-tagged human WT or T368A mutant SENP2 with p90RSK and detected exogenous SENP2 phosphorylation using anti–phospho–SENP2-T368. We found that SENP2-WT, but not the T368A mutant, was phosphorylated (Supplemental Figure 4A). In addition, we found that phosphorylation of human SENP2 was critical for p90RSK-mediated p53 SUMOylation, indicating the importance of T368 phosphorylation for both human and mouse SENP2 (Supplemental Figure 4B). We also confirmed T368 phosphorylation of endogenous SENP2 and found that this phosphorylation was completely abolished by Ad-DN-p90RSK (Figure 3E). To determine the role of p90RSK-mediated SENP2-T368 phosphorylation in p53 and ERK5 SUMOylation, we separately overexpressed SENP2 mutants in ECs using adenovirus vectors and found that only the SENP2-T368A mutant inhibited d-flow–induced p53 and ERK5 SUMOylation (Figure 4, A and B, and Supplemental Figure 4, C and D). We also found that d-flow–induced p53–Bcl-2 binding, which is a downstream event of p53 SUMOylation and is crucial for inducing apoptosis under d-flow (3), was significantly inhibited by Ad-SENP2-T368A mutant transduction (Figure 4A). Finally, d-flow–induced cleaved caspase–3 expression, inflammatory adhesion molecule expression, and reduced eNOS expression were significantly decreased by Ad-SENP2-T368A mutant transduction compared with Ad-SENP2-WT transduction (Figure 4, C and D). Taken together, these results suggest that SENP2-T368 phosphorylation is a key regulator of p53 and ERK5 SUMOylation and plays a critical role in d-flow–mediated EC apoptosis and inflammation.

p90RSK-SENP2 association is critical for p53 and ERK5 SUMOylation. To further investigate how p90RSK regulates SENP2, we sought to determine the specific SENP2-binding domain on p90RSK. Myc-tagged SENP2 coimmunoprecipitated

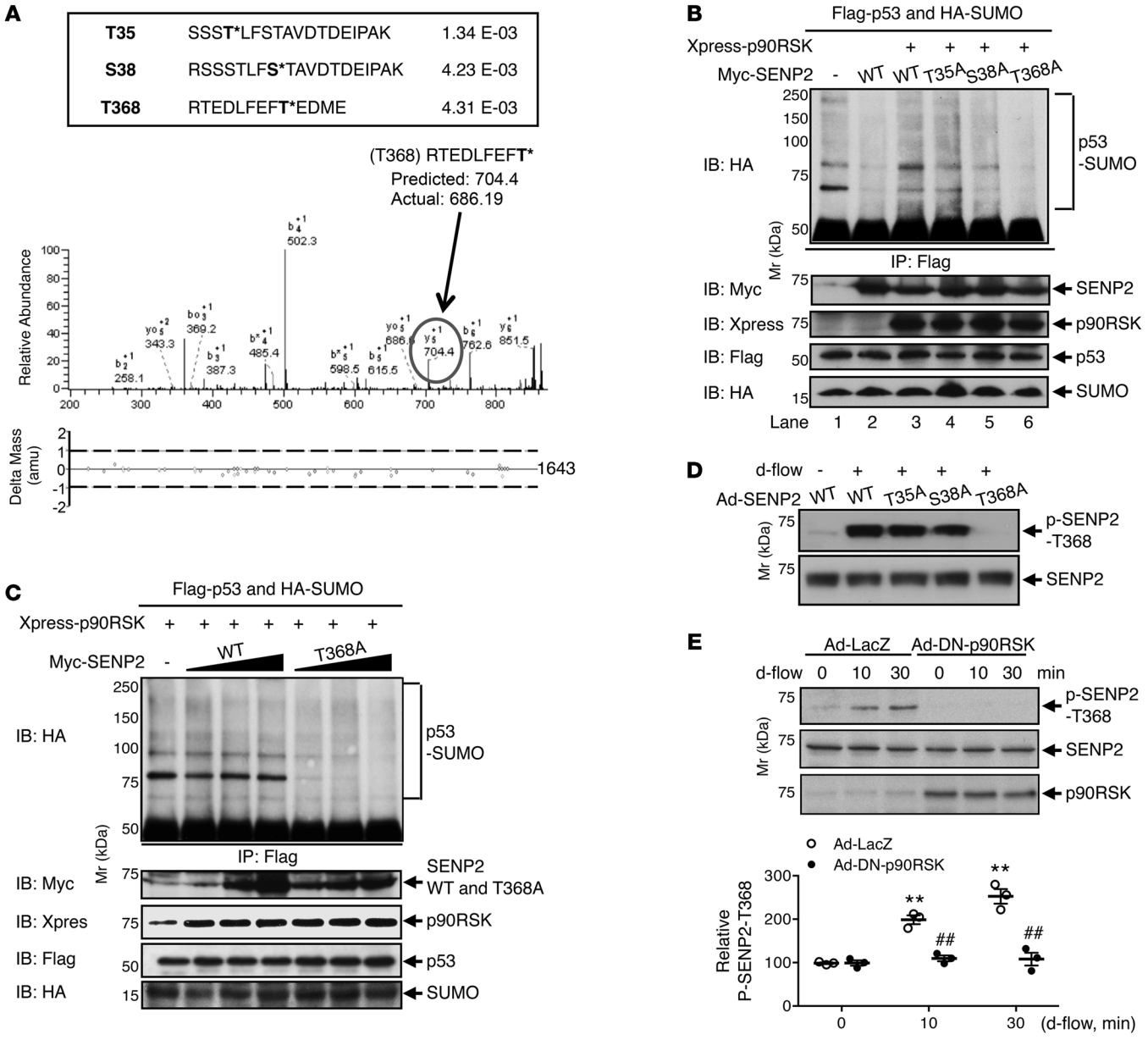

Figure 3. p90RSK-mediated SENP2-T368 phosphorylation is critical for p53 SUMOylation. (**A**) An LC-MS/MS analysis identified SENP2 phosphorylation sites by p90RSK at T35, S38, and T368 with a less than 0.05 error (upper panel). An LC-MS/MS plot of different peptide fragments shows T368 phosphorylation based on mass shift of phosphorylated threonine within H_2O (686 Da, lower panel). (**B** and **C**) CHO cells were cotransfected with 4 plasmids, Flag-p53, HA-SUMO3, Xpress-p90RSK1, and an additional plasmid containing one of the following pCS-Myc–tagged plasmids encoding SENP2-WT, SENP2-T35A, SENP2-S38A, or SENP2-T368A. Control plasmid contained only Flag-p53 and HA-SUMO. p53 SUMOylation was determined as described in Methods. p53, SUMO3, p90RSK, and SENP2 expression were detected by Western blotting. (**D**) HUVECs were transduced with Ad-SENP2-WT or SENP2 phosphorylation mutants as indicated and stimulated by d-flow or no flow (–) for 3 hours, and SENP2-T368 phosphorylation was detected using anti–phospho–SENP2-T368. (**B**–**D**) The blots shown are representative of 3 independent experiments. (**E**) After transduction of Ad-LacZ or Ad-DN-p90RSK, d-flow–induced SENP2-T368 phosphorylation was analyzed by Western blotting. Quantification of data represents mean ± SEM (lower panel, $n = 3$). $^{**}P < 0.01$, compared with no-flow conditions in the presence of Ad-LacZ; $^{\#\#}P < 0.01$, compared with each time point of Ad-LacZ control by 1-way ANOVA followed by Bonferroni's post hoc test.

Flag-tagged p90RSK (Figure 5A). We then used 4 different truncated mutants of SENP2 and found that SENP2-Fr.1 (1–130 aa) and SENP2-Fr.2 (131–300 aa) were able to interact with p90RSK in a mammalian 2-hybrid assay, which we had previously described (ref. 13 and Figure 5B). However, only overexpression of SENP2-Fr.2 inhibited p90RSK-SENP2 binding; it also inhibited p90RSK-mediated p53 SUMOylation (Supplemental Figure 5, A and B).

Next, we determined whether d-flow induced endogenous p90RSK-SENP2 binding and SENP2-T368 phosphorylation in HUVECs and found that d-flow stimulation for 20 to 40 minutes increased both binding and phosphorylation (Supplemental Figure 5C). Interestingly, d-flow–induced SENP2-T368 phosphorylation was inhibited by SENP2-Fr.2 overexpression (Figure 5C and Supplemental Figure 5A), suggesting that weak interaction of this

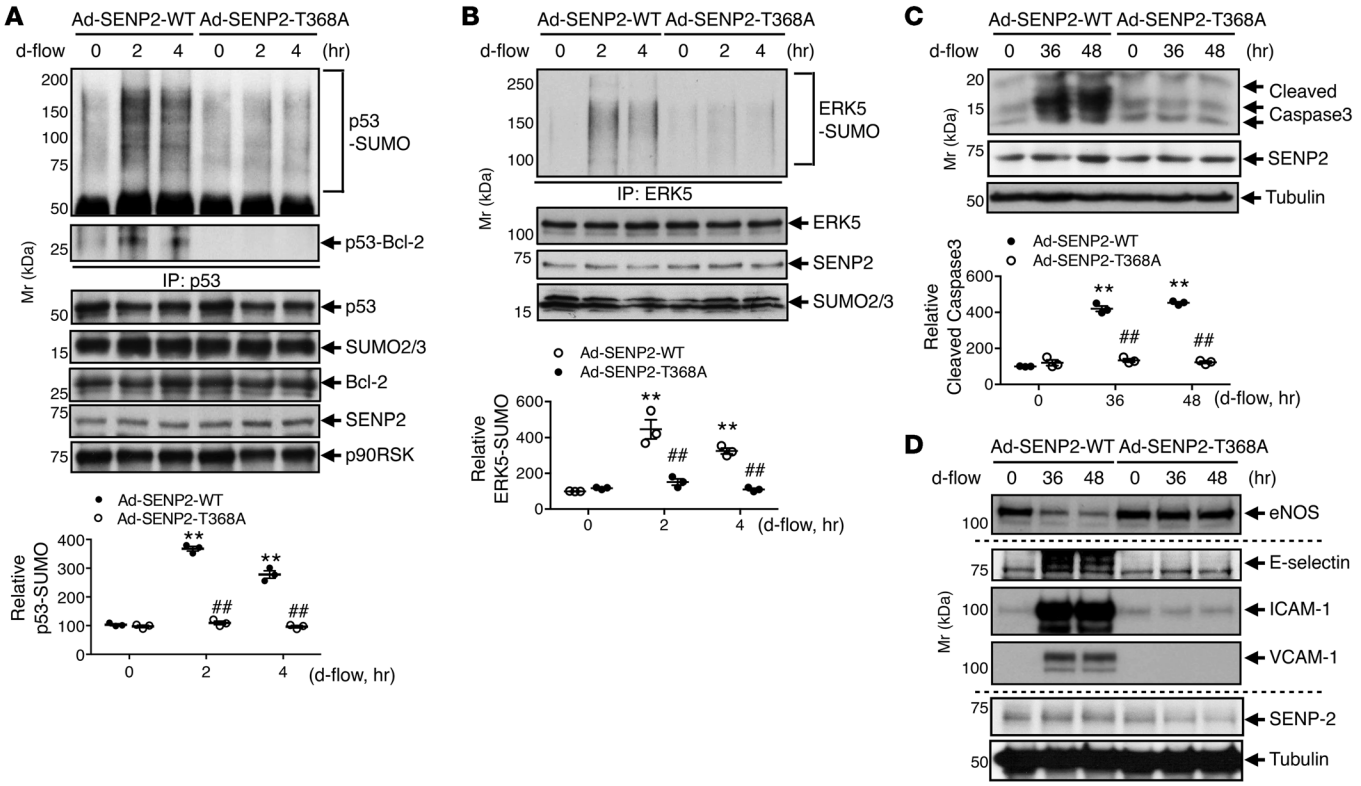

Figure 4. SENP2-T368 phosphorylation by p90RSK causes EC apoptosis and inflammation. After HUVECs were transduced with Ad-SENP2-WT or Ad-SENP2-T368A and exposed to d-flow as indicated, p53 and ERK5 SUMOylation (**A** and **B**), p53–Bcl-2 binding (**A**, middle panel), cleaved caspase-3 expression (**C**), and eNOS and adhesion molecule expression (**D**) were analyzed. (**A**–**C**) Quantification of data represents mean ± SEM (lower panel, $n = 3$). $^{**}P < 0.01$, compared with no-flow condition in the presence of Ad-SENP2-WT; $^{\#\#}P < 0.01$, compared with each time point of Ad-SENP2-WT control by 1-way ANOVA followed by Bonferroni's post hoc test.

domain with p90RSK is necessary for T368 phosphorylation. To see whether SENP2-T368 phosphorylation regulated d-flow–induced p90RSK-SENP2 association in cells, we transduced HUVECs with Ad-SENP2-WT, Ad-SENP2-T368A, or Ad-LacZ as a control and examined p90RSK-SENP2 binding. We found that d-flow increased SENP2-T368 phosphorylation and p90RSK-SENP2 binding in Ad-SENP2-WT and Ad-LacZ transduced cells, but not in SENP2-T368A mutant transduced cells (Figure 5D). Taken together, these results demonstrate a functional interplay between p90RSK-SENP2 binding and SENP2-T368 phosphorylation. In addition, d-flow–induced SUMOylation of p53 and ERK5 was abolished in HUVECs transduced with adenovirus containing SENP2-Fr.2 (Figure 5, E and F), suggesting a crucial role of direct binding between p90RSK and SENP2 in the regulation of SENP2 function.

d-flow induces SENP2 nuclear export via T368 phosphorylation. SENP2 contains a bipartite nuclear localization signal (NLS) sequence in the N terminus domain and a leucine-rich, CRM1-dependent nuclear export signal (NES) sequence in the central domain (ref. 15 and Figure 5B). These NLS and NES sequences are involved in SENP2 shuttling between the nucleus and the cytoplasm, which could regulate SENP2 function. To investigate the possibility that SENP2-T368 phosphorylation regulates SENP2 cellular localization, HUVECs were transduced with Ad-SENP2-WT or Ad-SENP2-T368A, and SENP2 localization was evaluated. Interestingly, d-flow increased SENP2-WT nuclear export, which was significantly inhibited by the T368A mutation (Figure 6A). To determine the role of SENP2 nuclear export and T368 phosphorylation in vivo, we investigated T368 phosphorylation-dependent SENP2 localization using en face aorta preparations and confocal microscopy (Figure 6, B and C). We focused on 2 areas: the region exposed to d-flow (lesser curvature of the aortic arch) and the area exposed to s-flow (greater curvature of the aortic arch), as we described previously (11, 16). When the endothelium was double-stained with anti-SENP2 or anti–phospho–SENP2-T368 together with anti–vascular endothelial-cadherin (anti–VE-Cad) as an EC marker, clear SENP2 nuclear localization was observed in the s-flow area. In the d-flow area, however, an increased level of anti-SENP2 extranuclear staining was observed (Figure 6B). In addition, although it was very low in the s-flow area, a robust increase in anti–phospho–SENP2-T368 staining was detected in the extranuclear compartment in d-flow areas (Figure 6C), indicating that T368 phosphorylation by d-flow is consistent with SENP2 nuclear export.

Role of p90RSK in EC inflammation and apoptosis and subsequent atherosclerotic plaque formation. To examine the role of p90RSK in EC pathology, aortas from male *Ldlr*$^{-/-}$ mice (7 weeks old) fed normal chow for 2 weeks were isolated and en face preparations were stained with anti-p90RSK and anti–phospho–p90RSK-S380. We found that both total p90RSK and phospho-p90RSK signals were significantly higher in the d-flow area compared with the s-flow area (Supplemental Figure 6). When these

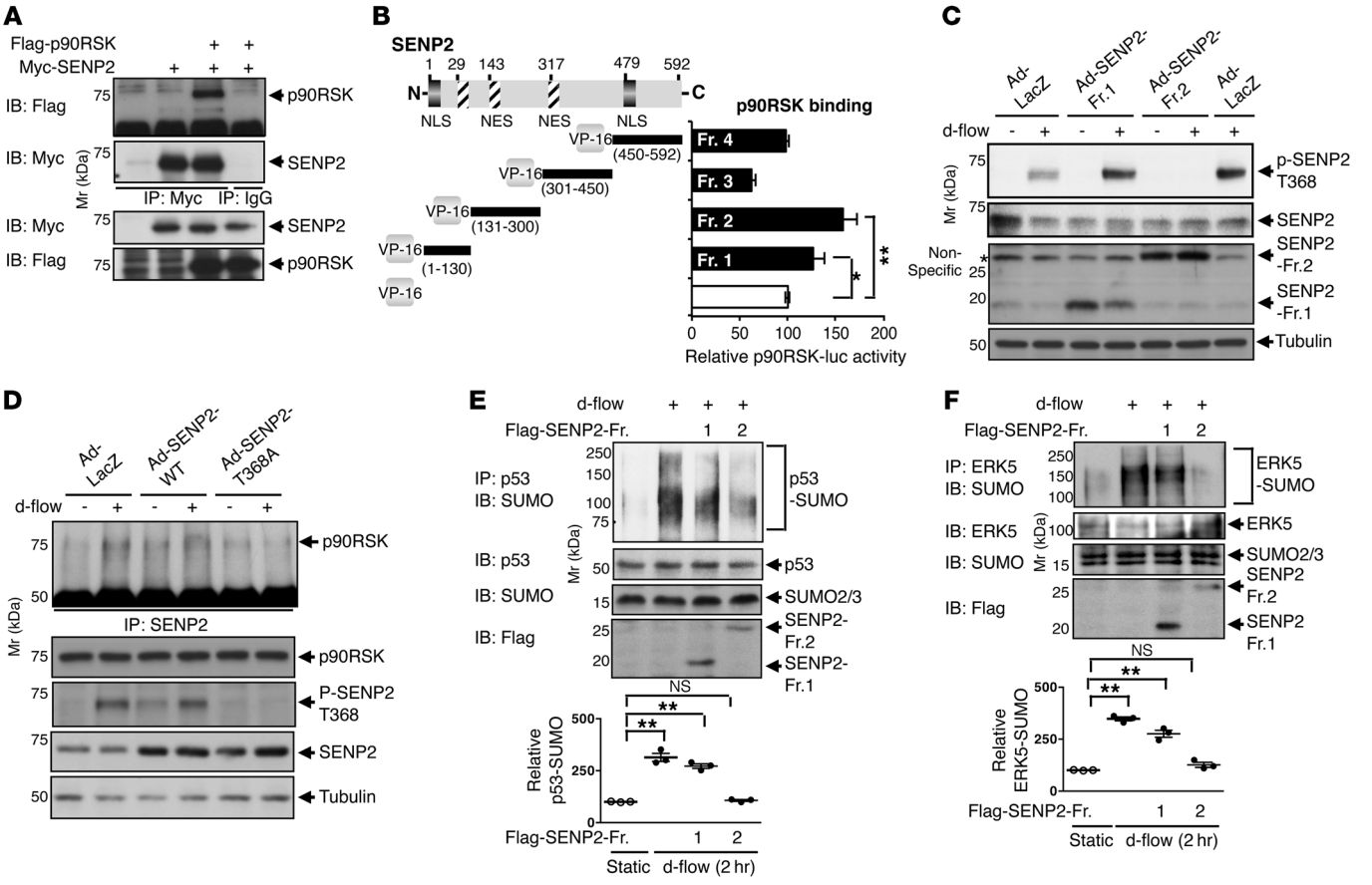

Figure 5. p90RSK-SENP2 association is critical for p53 and ERK5 SUMOylation. (**A**) HeLa cells were transfected with Myc-tagged SENP2 and Flag-tagged p90RSK and subjected to immunoprecipitation with anti-Myc or IgG (as a control) followed by Western blotting with anti-Flag or anti-Myc (first and second panel from top). (**B**) HUVECs were transfected with plasmids containing Gal4-p90RSK WT, indicated VP16-SENP2 fragments or empty vector, and Gal4-responsive luciferase reporter pG5-luc. After 24 hours of transfection, cells were stimulated with or without d-flow for 2 hours and luciferase activities were quantified. Data represent mean ± SEM (n = 3). $^*P < 0.05$; $^{**}P < 0.01$, by 1-way ANOVA followed by Bonferroni's post hoc test. (**C**) HUVECs were transduced with 50 MOI of adenoviruses of indicated SENP2 fragment mutants for 18 hours and then stimulated by d-flow for 30 minutes followed by Western blotting with anti–phospho–SENP2-T368, anti-SENP2, and anti-tubulin. (**D**) HUVECs were transduced with 50 MOI of indicated adenoviruses for 18 hours and then stimulated by d-flow for 30 minutes. SENP2 was immunoprecipitated and immunoblotted with anti-p90RSK. SENP2 phosphorylation at T368 and expression of p90RSK, SENP2, and tubulin were examined using specific antibodies. (**A**–**D**) The blots or quantified data (mean ± SEM) shown are representative of 3 independent experiments. (**E** and **F**) d-flow–induced p53 and ERK5 SUMOylation were detected after transduction of Ad-SENP2 Fr.1, Ad-SENP2 Fr.2, or Ad-LacZ as a control. Quantification of data represents mean ± SEM (lower panel, n = 3). $^{**}P < 0.01$, by 1-way ANOVA followed by Bonferroni's post hoc test.

mice were fed a high-fat diet (HFD) for 2 weeks, significantly increased staining was observed in both d- and s-flow areas compared with the normal chow-fed group (Supplemental Figure 6). These data suggest that atherogenic environment (i.e., HFD) induces not only activation but also expression of p90RSK and further increases d-flow–induced SENP2-T368 phosphorylation in vivo. To specifically study the role of p90RSK in ECs in vivo, we generated EC-specific WT-*p90rsk* transgenic mice using mice expressing tamoxifen-inducible *Cre*-recombinase *CreER*^{T2} under the regulation of the *VE-Cad* promoter (17) (*VE-Cad-Cre* Tg [WT-*p90rsk*^{fl}], herein referred to as WT-*p90rsk*-ETg). We expressed WT-*p90rsk*, as opposed to a constitutively active mutant form of p90RSK, because a portion of overexpressed WT-*p90rsk* is constitutively active, as shown in Figure 1. As controls, we used nontransgenic littermates (NLC: *VE-Cad-Cre*$^{+/-}$ Tg[WT-*p90rsk*] or *VE-Cad-Cre*$^{-/-}$ Tg[WT-*p90rsk*^{fl}]) that did not express exogenous p90RSK under 4-hydroxytamoxifen (4-OHT) treatment. We did not find any phenotypic differences between these 2 strains of NLC (data not shown). SENP2-T368 phosphorylation, expression of inflammatory adhesion molecules at both protein and mRNA levels, and cleaved caspase-3 expression were increased in mouse ECs (MECs) isolated from WT-*p90rsk*-ETg compared with those from NLC mice after 4-OHT injection (Figure 7, A and B). In contrast, eNOS expression was downregulated in the WT-*p90rsk*-ETg mice (Figure 7A). To examine the role of p90RSK in atherogenesis, we generated WT-*p90rsk*-ETg/*Ldlr*$^{-/-}$ mice and compared the extent of atherogenesis in these mice with that in NLC/*Ldlr*$^{-/-}$ mice after 16 weeks on a high-cholesterol diet. Differences were noted in their body weight and blood measurements of total, LDL, and HDL cholesterol (Supplemental Figure 7, A and B). The lesion areas in both aortic arch and descending aorta were significantly larger in WT-*p90rsk*-ETg/*Ldlr*$^{-/-}$ than in NLC/*Ldlr*$^{-/-}$ mice (Figure 7C). We also found that the lesion size at the level of the aortic valve was larger in WT-*p90rsk*-ETg /*Ldlr*$^{-/-}$ than in NLC/*Ldlr*$^{-/-}$ mice (Figure 7D).

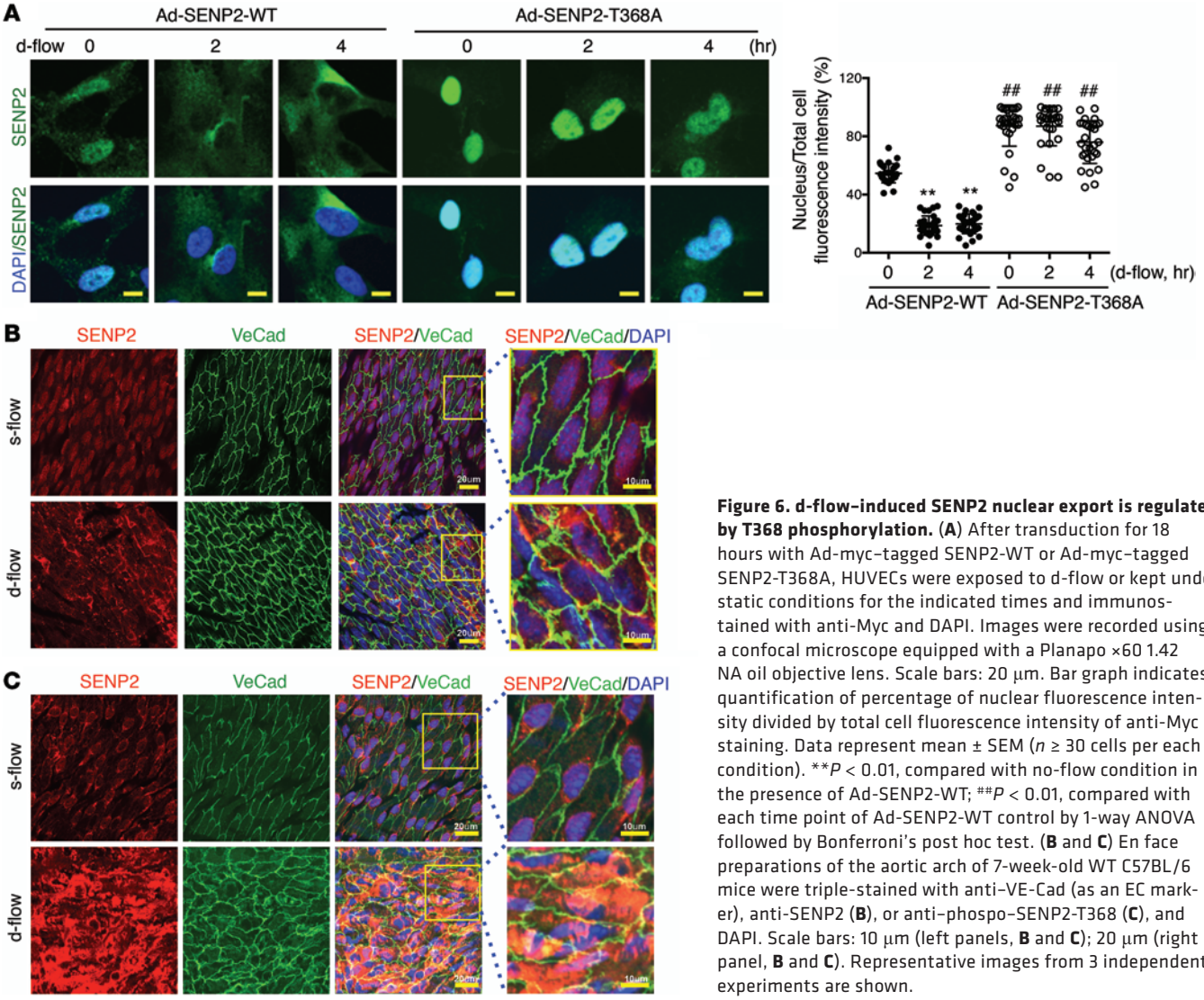

Figure 6. d-flow–induced SENP2 nuclear export is regulated by T368 phosphorylation. (**A**) After transduction for 18 hours with Ad-myc–tagged SENP2-WT or Ad-myc–tagged SENP2-T368A, HUVECs were exposed to d-flow or kept under static conditions for the indicated times and immunostained with anti-Myc and DAPI. Images were recorded using a confocal microscope equipped with a Planapo ×60 1.42 NA oil objective lens. Scale bars: 20 μm. Bar graph indicates quantification of percentage of nuclear fluorescence intensity divided by total cell fluorescence intensity of anti-Myc staining. Data represent mean ± SEM ($n \geq 30$ cells per each condition). $^{**}P < 0.01$, compared with no-flow condition in the presence of Ad-SENP2-WT; $^{\#\#}P < 0.01$, compared with each time point of Ad-SENP2-WT control by 1-way ANOVA followed by Bonferroni's post hoc test. (**B** and **C**) En face preparations of the aortic arch of 7-week-old WT C57BL/6 mice were triple-stained with anti–VE-Cad (as an EC marker), anti-SENP2 (**B**), or anti–phospo-SENP2-T368 (**C**), and DAPI. Scale bars: 10 μm (left panels, **B** and **C**); 20 μm (right panel, **B** and **C**). Representative images from 3 independent experiments are shown.

Role of the p90RSK-SENP2 module in atherosclerotic plaque formation. To establish the role of the p90RSK-SENP2 module in d-flow–elicited apoptosis and inflammation, we generated EC-specific dominant-negative p90RSK transgenic (*VE-Cad-Cre*$^{+/-}$ Tg[DN-*p90rsk*^{fl}]; herein referred to as DN-*p90rsk*-ETg) mice and also double-transgenic/knockout mice (DN-*p90rsk*-ETg/*Senp2*$^{+/-}$). Of note, we have already reported increased apoptosis and inflammatory adhesion molecule expression in both s- and d-flow areas in the aortic arch in *Senp2*$^{+/-}$ mice (11). The extent of apoptosis (Supplemental Figure 8, A and B) and VCAM-1 expression (Figure 8A) in the d-flow area in the aortic arch was significantly dampened in DN-*p90rsk*-ETg mice, but these antiatherogenic phenotypes were lost in the double-transgenic mice. d-flow–induced SENP2-T368 phosphorylation (Figure 8B), adhesion molecule expression (Figure 8C), and cleaved caspase-3 expression (Figure 8C) were also reduced in MECs isolated from DN-*p90rsk*-ETg mice, but in MECs isolated from DN-*p90rsk*-ETg/*Senp2*$^{+/-}$ mice, DN-p90RSK–mediated inhibition of adhesion molecule expression and apoptosis was completely reversed.

Next, to explore whether d-flow–mediated p90RSK activation was involved in atherogenesis, we made partial ligation of left carotid artery (PLCA) models using NLC/*Ldlr*$^{-/-}$, DN-*p90rsk*-ETg/*Ldlr*$^{-/-}$, and DN-*p90rsk*-ETg/*Senp2*$^{+/-}$/*Ldlr*$^{-/-}$ mice. The mouse PLCA model has been used to experimentally generate an area of d-flow where atherogenic responses are induced in a short period of time (18–20). There was no notable difference in cholesterol levels among these mice after 4-OHT injection and partial ligation (Supplemental Figure 9). Intimal lesion formation and lipid deposition were inhibited in DN-*p90rsk*-ETg/*Ldlr*$^{-/-}$ mice, but these inhibitions were completely abolished in DN-*p90rsk*-ETg/*Senp2*$^{+/-}$/*Ldlr*$^{-/-}$ mice (Figure 9, A–E, and Supplemental Figure 10A). Next, to determine the contribution of macrophages and vascular smooth muscle cells to lesion formation, we performed cell type–specific staining using anti-MAC3 (macrophages) and anti–α-smooth muscle actin (α-SMA) (smooth muscle cells). We found accumulation of anti-MAC3–staining cells, but not α-SMA–staining cells, in the intima of NLC/*Ldlr*$^{-/-}$ and DN-*p90rsk*-ETg/*Senp2*$^{+/-}$/*Ldlr*$^{-/-}$ mice. However, this inflammatory cell infiltration into the lesion was significantly impaired in

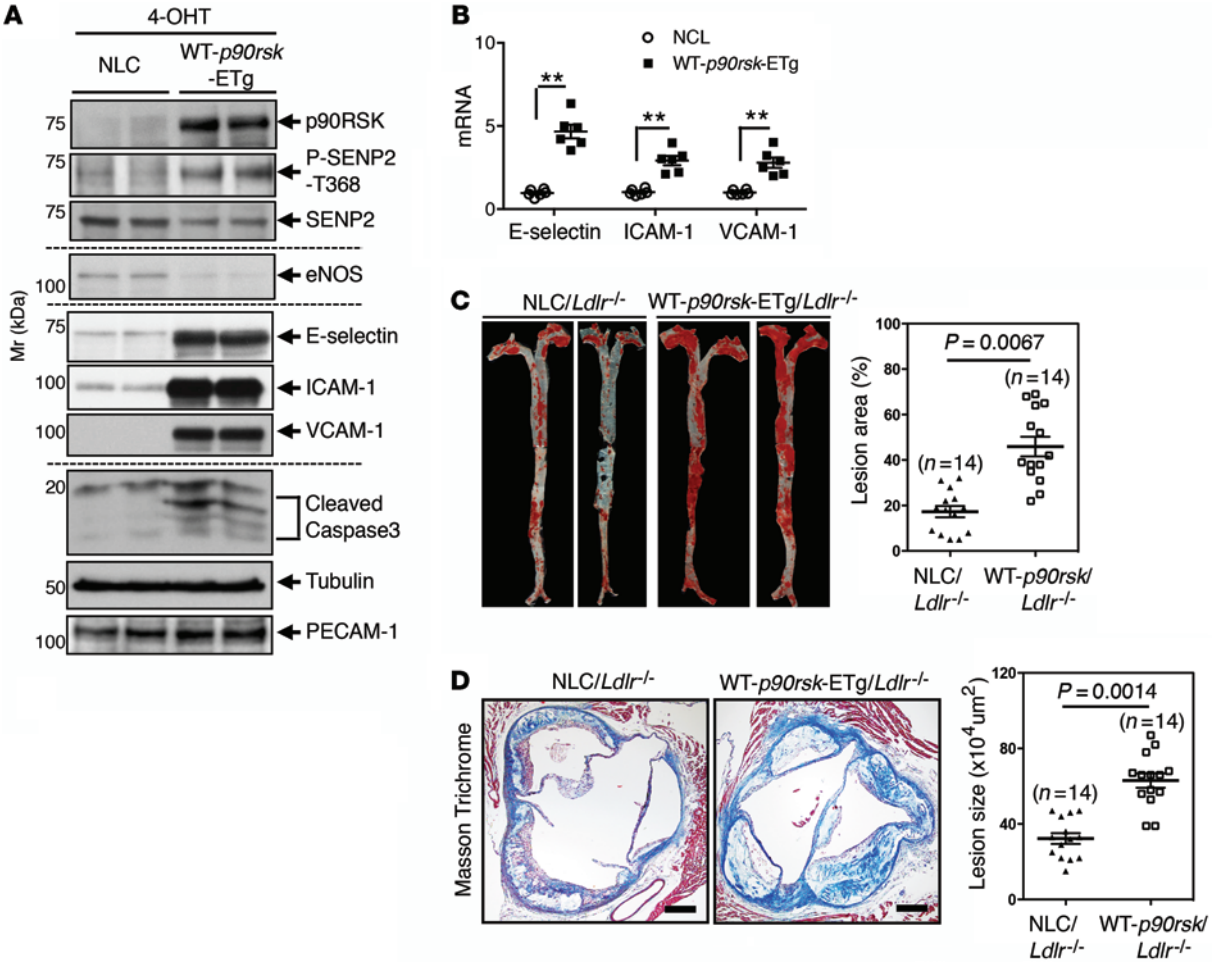

Figure 7. Role of p90RSK in EC inflammation and apoptosis and atherosclerotic plaque formation. SENP2-T368 phosphorylation, protein levels of adhesion molecules, cleaved caspase-3, and eNOS (**A**), and mRNA levels of adhesion molecules (**B**) in MECs isolated from WT-*p90rsk*-ETg mice are shown. Data represent mean ± SEM (n = 6). $^{**}P < 0.01$, by Student's t test. (**C** and **D**) NLC/*Ldlr*$^{-/-}$ and WT-*p90rsk*-ETg/*Ldlr*$^{-/-}$ mice were given a high-cholesterol diet for 16 weeks. WT-*p90rsk*-ETg/*Ldlr*$^{-/-}$ mice exhibited increased oil red O–stained atherosclerotic lesions in the whole aorta as well as increased Masson's trichrome–stained atherosclerotic lesions in the aortic valve region. Scale bars: 100 μm. Quantified en face (**C**) and histology (**D**) data are shown. Data represent mean ± SEM (n = 14 for each genotype). P = 0.0067; P = 0.0014, by Student's t test.

DN-*p90rsk*-ETg/*Ldlr*$^{-/-}$ mice (Supplemental Figure 10, B and C). These results demonstrate that the p90RSK-SENP2 module in ECs plays a critical role in d-flow–induced atherogenesis.

Discussion

In this study, we provide evidence that p90RSK, a key activator of d-flow–induced EC dysfunction and subsequent development of atherosclerosis, is a downregulator of the SENP2 de-SUMOylation function on p53 and ERK5. We have shown that d-flow activates p90RSK and phosphorylates SENP2-T368, which was identified as a phosphorylation site of this SUMO protease in this study. Phosphorylated SENP2 loses its de-SUMOylation function and, as a result, SUMOylation levels of p53 and ERK5 increase, causing EC dysfunction.

Chronic low-grade inflammation and apoptosis are thought to induce EC dysfunction and atherosclerosis (11, 13). We have previously published that d-flow induces ERK5 and p53 SUMOylation, which leads to EC inflammation and apoptosis (11). Unlike d-flow stimulation, SUMOylation of p53 and ERK5 was downregulated by s-flow and the level of this downregulation went below the level of SUMOylation in cells kept under static conditions (11). In addition, we have already reported that s-flow increased and d-flow decreased ERK5 transactivation via regulating ERK5-SUMOylation (8, 11). These data suggest crucial roles played by p53 and ERK5 SUMOylation in differentiating EC responses to s-flow and d-flow.

Our present study has uncovered the central role of the p90RSK-SENP2 module in d-flow–elicited EC signaling that leads to vascular dysfunction. This conclusion is based on several findings, including that (a) p90RSK regulates SENP2 de-SUMOylation function by phosphorylating SENP2-T368, (b) p90RSK-mediated SENP2-T368 phosphorylation modulates the function of p53 and ERK5, and (c) endothelial p90RSK activation by d-flow induces EC inflammation, apoptosis, and subsequent atherosclerotic plaque formation. In *Ldlr*$^{-/-}$ mice, a conventional atherosclerosis model, not only d-flow–induced endothelial dysfunction but also many other factors, including macrophage- and lymphocyte-mediated inflammation, contribute to atherogenesis. In contrast,

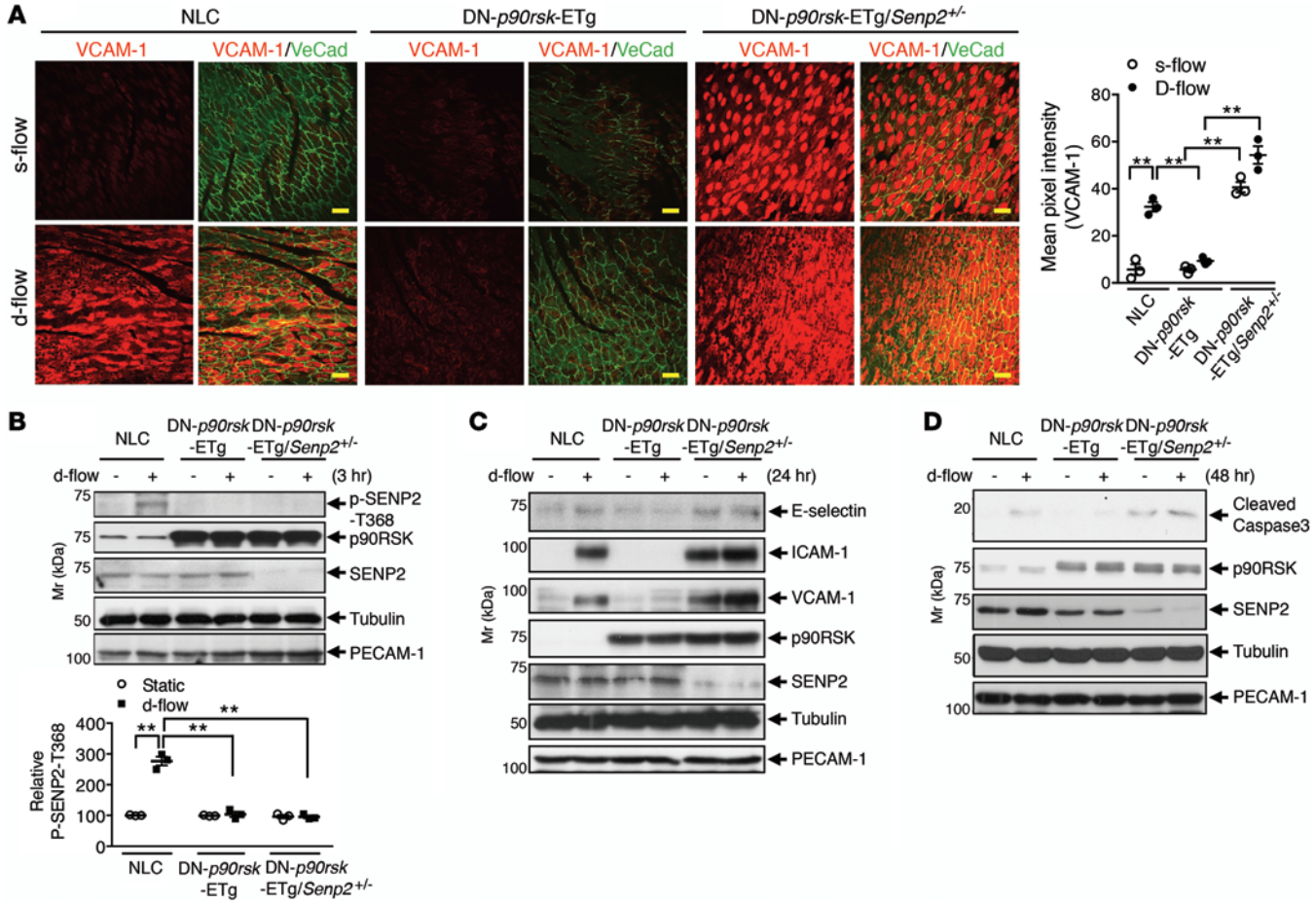

Figure 8. Role of the p90RSK-SENP2 module in d-flow–elicited inflammation and apoptosis. (**A**) En face preparations of aortic arch of 7-week-old NLC, DN-*p90rsk*-ETg, or DN-*p90rsk*-ETg/*Senp2*$^{+/-}$ mice were double-stained with anti–VE-Cad and anti–VCAM-1. Scale bars: 20 μm. The graph shows anti–VCAM-1 staining intensities in d- and s-flow areas of the aortic arch. Data represent mean ± SEM. Right panel, $n = 3$ for each genotype. $^{**}P < 0.01$, by 1-way ANOVA followed by Bonferroni's post hoc test. (**B**–**D**) MECs isolated from NLC, DN-*p90rsk*-ETg, or DN-*p90rsk*-ETg/*Senp2*$^{+/-}$ mice were stimulated with d-flow, and SENP2-T368 phosphorylation (**B**), expression of adhesion molecules as inflammation markers (**C**), and cleaved caspase-3 expression as an apoptosis marker (**D**) were determined by Western blotting. (**B**) Bar graph shows the quantification of SENP2-T368 phosphorylation levels after normalization with tubulin expression. Data represent mean ± SEM ($n = 3$ for each genotype). $^{**}P < 0.01$, by 1-way ANOVA followed by Bonferroni's post hoc test. (**C** and **D**) The blots shown represent 1 of 3 independent experiments.

the PLCA model allows one to study the role of d-flow regardless of other factors, including genetic backgrounds of animals, and it is now a well-accepted atherosclerosis model (18–20). Therefore, to obtain direct evidence for the cause and effect relationship between d-flow and atherosclerosis, we chose this model. Robust formation of lipid lesions in this model has been reported (18–20), which supports the concept of d-flow–induced atherosclerosis. To confirm this observation, we performed oil red O staining and found significant lipid deposition in the intima of LCA after partial ligation (Figure 9D). Next, to determine the contribution of macrophages and vascular smooth muscle cells to lesion formation, we performed cell type–specific staining using anti-MAC3 (macrophages) and anti–α-SMA (smooth muscle cells). Although we identified some vascular smooth muscle cells in the plaque, the majority of cells were Mac3 positive (Supplemental Figure 10B), which showed very different phenotypes from those observed in vascular remodeling and neointima formation after PLCA in non-*Ldlr*$^{-/-}$ or *Apoe*$^{-/-}$ mice on a regular chow diet (21). Previously, we have reported that *Ldlr*$^{-/-}$ mice that received *Senp2*$^{+/-}$ hematopoietic cells by bone marrow transplantation showed the same extent of vascular lesion development in the aortic root as the mice given cells from *Senp2*$^{+/+}$ donors, suggesting that vascular SENP2 expression regulates atherosclerosis plaque formation (11). In addition, we found a significant increase in endothelial inflammation in *Senp2*$^{+/-}$ mice in vivo (11). Taken together, these data suggest that EC damage, but not macrophage or vascular smooth muscle cell proliferation, is the main mechanism of this lesion formation.

The concept that p90RSK-SENP2 compartmentalization (nucleus vs. cytosol), which regulates SENP2 function, is critical for the regulation of atherogenesis is, we believe, novel and highlights the importance of SUMOylation in mechanotransduction of d-flow that dictates the initial development of atherosclerotic plaques. The proteins we have focused on in this study should be attractive drug targets, since they are uniquely involved in signaling events that are activated by d-flow. We have shown that p90RSK-mediated SENP2-T368 phosphorylation plays a central role in endothelial inflammation and apoptosis, which are causally tied to diseases such as hypertension, diabetes, and coronary

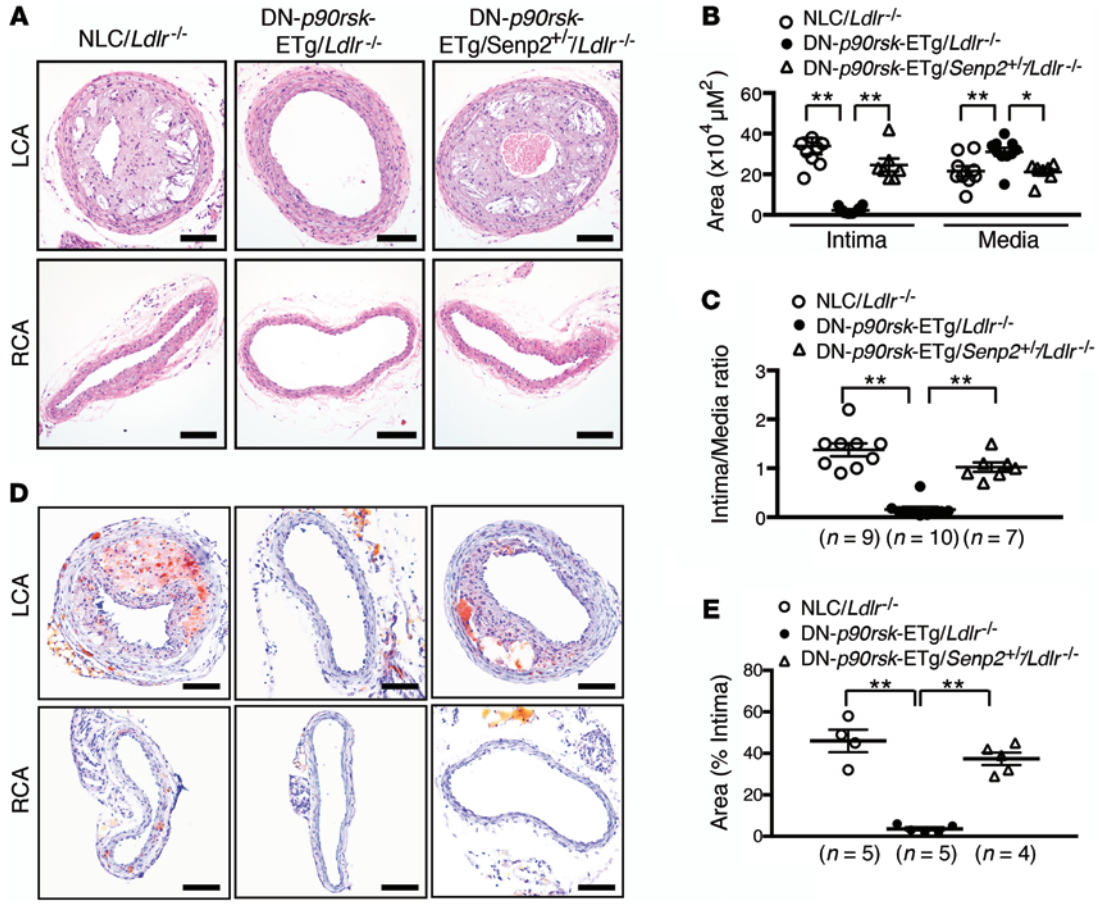

Figure 9. Role of the p90RSK-SENP2 module in atherosclerotic plaque formation. (**A**) Atherosclerotic lesions 4 weeks after partial left carotid artery (LCA) ligation in NLC/*Ldlr*$^{-/-}$ (n = 9), DN-*p90rsk*-ETg/*Ldlr*$^{-/-}$ (n = 10), and DN-*p90rsk*-ETg/*Senp2*$^{+/-}$/*Ldlr*$^{-/-}$ (n = 7) mice are shown. Unligated right carotid artery (RCA) in each mouse is used as control. Representative images are shown after H&E staining. Scale bars: 50 μm. The intimal lesion area and the media area (**B**), and the intima/media ratio (**C**) were determined in cross-sections of ligated LCAs. Data represent mean ± SEM. *P < 0.05; **P < 0.01, by 1-way ANOVA followed by Bonferroni's post hoc test. (**D**) Representative images of frozen sections of LCA and RCA after LCA ligation are shown with oil red O staining displaying lipid deposits. Scale bars: 50 μm. (**E**) Bar graph shows quantification of oil red O–stained areas in the intima of NLC/*Ldlr*$^{-/-}$ (n = 4), DN-*p90rsk*-ETg/*Ldlr*$^{-/-}$ (n = 5), and DN-*p90rsk*-ETg/*Senp2*$^{+/-}$/*Ldlr*$^{-/-}$ (n = 5) mice. Data represent mean ± SEM. **P < 0.01, by 1-way ANOVA followed by Bonferroni's post hoc test.

artery diseases. As such, this d-flow–mediated SUMOylation pathway provides what we believe is a new insight into therapeutic approaches for the prevention of these diseases.

Methods

Additional details of experimental procedures are included in Supplemental Methods.

Generation of mouse anti–phospho–SENP2-T368. A peptide corresponding to the aa sequence from 358 to 378 of mouse SENP2 (Biotin-NPEGQ-DRRTEDLFEFT*EDMEKEISNA) was synthesized (Peptibody Inc.) with an aminoterminus biotin label in both phosphorylated and unphosphorylated forms. A mouse anti–phospho–SENP2-T368 single-chain Fv (scFv) was generated against the phospho-peptide by phage display (22) with a naive human phage display library constructed from peripheral blood lymphocytes (23, 24).

Isolation of MECs. MECs were isolated according to our previous publication (1).

Cell culture and flow apparatus. HUVECs were obtained from collagenase-digested umbilical cord veins (25) and collected in M200 medium supplemented with LSGS (Cascade Biologic) and 5% fetal bovine serum (Hyclone). HUVECs were cultured on 0.2% gelatin-precoated dishes. Cells were used for experiments at passages 4 and 5. To expose the cells to flow in vitro, we used a cone-and-plate flow apparatus described previously (26). Confluent cells cultured in 100-mm dishes were exposed to s-flow (shear stress = 20 dyn/cm^2) or d-flow created by a cone with radial grooves as we described previously (7). HeLa, human cervical adenocarcinoma (no. CCL2), and CHO, hamster ovary (no. CCL-61), cell lines used in this study were purchased from ATCC.

Immunoprecipitation (SUMO assay) and Western blot analysis. Cells were collected in PBS containing 10 mM N-ethylmaleimide (NEM), and cell extracts were prepared in modified radioimmunoprecipitation assay (RIPA) buffer. SUMOylation was detected as previously described (7).

In vitro phosphorylation of SENP2 by activated p90RSK. Glutathione-*S*-transferase–SENP2–truncated (GST–SENP2–truncated) mutant proteins were expressed in *Escherichia coli*, purified with glutathione–sepharose 4B as described (Pharmacia Biotech Inc.), and used in in vitro kinase assays with activated p90RSK, as described previously (27).

Mammalian 2-hybrid analysis and transfection of cells. Cells were plated in 12-well plates at 5 × 10^4 cells/well. The mammalian 2-hybrid assay was performed as described previously (4).

Real-time PCR assay. Total RNA was extracted using the TRIzol reagent according to the manufacturer's instructions. The reverse transcriptase reaction (PCR) was performed in 20 ml mixtures containing 1 μg of total RNA according to the manufacturer's protocol (no. 170-8890; Bio-Rad).

Analysis of apoptosis. In accordance with recently published guidelines, apoptosis was quantified by 2 methodologically unrelated criteria (28). Late-stage apoptosis was quantified by counting cells with positive TUNEL staining (29).

Animals. Tamoxifen-inducible (4-OHT) EC-specific transgenic mice and WT-*p90rsk* (WT-*p90rsk*-ETg) and dominant-negative p90rsk (K94A/K447A; DN-*p90rsk*-ETg) mice were generated by using mice expressing tamoxifen-inducible *Cre*-recombinase *Cre-ER*^{T2} under the regulation of the *VE-Cad* promoter (17) (provided by M. Luisa Iruela-Arispe, UCLA, Los Angeles, California, USA) (13). All mice were maintained under pathogen-free conditions at the Aab Cardiovascular Research Institute at the University of Rochester.

En face immunostaining. The s-flow and d-flow areas within the aorta were identified based on the published and generally accepted anatomical locations where such flow patterns are known to occur (3, 11). We performed en face staining as described in our previous reports (3, 4).

Partial carotid ligation and atherosclerosis. Partial carotid ligation has been well established as a model of d-flow–induced atherosclerosis, and we performed this surgery as previously described (30). Briefly, NLC/*Ldlr*$^{-/-}$, DN-*p90rsk*-ETg/*Ldlr*$^{-/-}$, and DN-*p90rsk*-ETg/*Senp2*$^{+/-}$/*Ldlr*$^{-/-}$ mice were anesthetized by 2.0% isoflurane, placed on a heated surgical pad, and subcutaneously given 2.5 mg/kg flunixin. Isoflurane was maintained at a level between 1.0% and 2.0%. After hair removal, a midline cervical incision was made and the internal and external carotid arteries were exposed and partially ligated with 6.0 silk suture, leaving the occipital artery patent. The skin was sutured with absorbable 6.0 silk suture in a running subcuticular pattern. Mice were allowed to recover in a clean cage on a heated pad. For the atherosclerosis study, mice were fed a HFD (TD88137, Harlan Laboratories) for 4 weeks, at which time their carotid arteries were harvested. To determine atherosclerotic lesions in histological sections, right (control) and left (surgery performed) carotid arteries were dissected out and all tissues were fixed in 10% neutralized formaldehyde solution. The fixed tissues were embedded in paraffin or OCT solution to cut frozen sections. Serial sections (5 μm) were made through the entire carotid arteries and stained with Masson's trichrome or H&E. To quantify neointima, H&E-stained carotid arteries were cross-sectioned, and the neointima area was calculated by subtracting the lumen area from the area circumscribed by the internal elastic lamina. The medial area was determined by the area between the internal and external elastic laminae. These measurements were made by using Image J 1.45 (http://imagej.nih.gov/ij/). The positions of internal and external elastic laminae were also confirmed by Masson's trichrome staining. The extent of neointimal thickening was determined by the neointima/media ratio. Frozen cross-sections of 10 μm were prepared from carotid arteries preserved in OCT medium for oil red O staining. Sections were air dried, fixed in ice-cold 10% formalin, and then rinsed in distilled water followed by staining with oil red O. Stained slides were analyzed under an Olympus microscope for accumulation of lipids.

Tissue preparation, histology, and quantification of the lesion size in the artery and aortic valve. NLC/*Ldlr*$^{-/-}$ or WT-*p90rsk*-ETg/*Ldlr*$^{-/-}$ female mice were injected with 4-OHT at 2 mg/mouse/d for 5 consecutive days followed by feeding a high-cholesterol diet (D01061401C, Research Diets) for 16 weeks. Mice were sacrificed by CO_2 inhalation at the end of the high-cholesterol–diet feeding. The arterial tree was perfused via the left ventricle with saline containing heparin (40 USPU/ml), followed by formaldehyde (10%, pH 7.3) in PBS for 10 minutes. The full-length of the aorta to the iliac bifurcation was dissected out and opened along the ventral midline. En face preparations were washed in distilled water, dipped in 60% isopropyl-alcohol, and stained for 40 minutes in 0.16% oil red O dissolved in 60% isopropyl-alcohol/0.2 mol/l NaOH. Stained images were captured with a digital camera mounted on an Olympus stereomicroscope and analyzed using Adobe Photoshop Extended software. Stained plaque areas were quantified blindly using ImageJ 1.45. To examine atherosclerotic lesions in the aortic valve area in histological sections, the aortic sinus area attached to the heart was dissected and then processed to make paraffin sections. Serial sections (5 μm) were made through the entire aortic valve and stained with H&E. To quantify the extent of total atherosclerotic lesion area in the aortic arch (11) and the intimal lesion and medial areas of the arterial wall (19, 31), image analysis was performed using ImageJ 1.45.

Cholesterol level analysis. Mice were anesthetized and blood samples were collected from the abdominal artery. Serum was prepared and total cholesterol, HDL, and non-HDL (LDL and VLDL) concentrations were measured enzymatically using commercially available kits (ab65390; Abcam). The assays were performed in accordance with the manufacturer's instructions.

Statistics. Data are presented as mean ± SEM. Differences between 2 independent groups were determined by Student's *t* test (2-tailed), and where applicable, 1-way ANOVA followed by Bonferroni's post hoc test for multiple group comparisons using GraphPad Prism 5.0 (GraphPad Software Inc.). When groups showed unequal variances, we applied Welch's ANOVA to perform multiple group comparisons. *P* values of less than 0.05 were accepted as being statistically significant.

Study approval. All animal procedures were approved by the University Committee on Animal Resources of the University of Rochester (approval no. 2007-091/100593).

Acknowledgments

We are grateful to Craig Morrell and Deanne M. Mickelsen for performing microsurgery on mice and for discussions and comments on the manuscript. This work is supported by grants HL-088637, HL-064839, and HL-077789 (to J. Abe); 12SDG11690003 and HL-118462A (to K.S. Heo); 11GRNT5850001 (to K. Fujiwara); and GM-071434 (to J. Taunton).

Address correspondence to: Jun-ichi Abe, Aab Cardiovascular Research Institute and Department of Medicine, University of Rochester School of Medicine and Dentistry, 601 Elmwood Ave., Box CVRI, Rochester, New York 14642, USA. Phone: 585.276.9794; E-mail: Jun-ichi_Abe@urmc.rochester.edu.

Chang-Hoon Woo's present address is: Department of Pharmacology, College of Medicine, Yeungnam University, Daegu, South Korea.

Kyung-Sun Heo, Nhat-Tu Le, Keigi Fujiwara, and Jun-ichi Abe's present address is: Department of Cardiology, Division of Internal Medicine, University of Texas MD Anderson Cancer Center, Houston, Texas, USA.

1. Libby P. Inflammation in atherosclerosis. *Nature*. 2002;420(6917):868–874.
2. Lusis AJ. Atherosclerosis. *Nature*. 2000;407(6801):233–241.
3. Heo KS, et al. PKCzeta mediates disturbed flow-induced endothelial apoptosis via p53 SUMOylation. *J Cell Biol*. 2011;193(5):867–884.
4. Heo KS, Fujiwara K, Abe J. Disturbed-flow–mediated vascular reactive oxygen species induce endothelial dysfunction. *Circ J*. 2011;75(12):2722–2730.
5. Malek AM, Alper SL, Izumo S. Hemodynamic shear stress and its role in atherosclerosis. *JAMA*. 1999;282(21):2035–2042.
6. Chang E, et al. MK2 SUMOylation regulates actin filament remodeling and subsequent migration in endothelial cells by inhibiting MK2 kinase and HSP27 phosphorylation. *Blood*. 2011;117(8):2527–2537.
7. Yu J, et al. RhoGDI SUMOylation at Lys-138 increases its binding activity to Rho GTPase and its inhibiting cancer cell motility. *J Biol Chem*. 2012;287(17):13752–13760.
8. Woo CH, et al. Extracellular signal-regulated kinase 5 SUMOylation antagonizes shear stress-induced antiinflammatory response and endothelial nitric oxide synthase expression in endothelial cells. *Circ Res*. 2008;102(5):538–545.
9. Hilgarth RS, Murphy LA, Skaggs HS, Wilkerson DC, Xing H, Sarge KD. Regulation and function of SUMO modification. *J Biol Chem*. 2004;279(52):53899–53902.
10. Geiss-Friedlander R, Melchior F. Concepts in sumoylation: a decade on. *Nat Rev Mol Cell Biol*. 2007;8(12):947–956.
11. Heo KS, et al. De-SUMOylation enzyme of sentrin/SUMO-specific protease 2 regulates disturbed flow-induced SUMOylation of ERK5 and p53 that leads to endothelial dysfunction and atherosclerosis. *Circ Res*. 2013;112(6):911–923.
12. Nigro P, et al. PKCzeta decreases eNOS protein stability via inhibitory phosphorylation of ERK5. *Blood*. 2010;116(11):1971–1979.
13. Le NT, et al. A crucial role for p90RSK-mediated reduction of ERK5 transcriptional activity in endothelial dysfunction and atherosclerosis. *Circulation*. 2013;127(4):486–499.
14. Le NT, et al. p90RSK targets the ERK5-CHIP ubiquitin E3 ligase activity in diabetic hearts and promotes cardiac apoptosis and dysfunction. *Circ Res*. 2012;110(4):536–550.
15. Itahana Y, Yeh ET, Zhang Y. Nucleocytoplasmic shuttling modulates activity and ubiquitination-dependent turnover of SUMO-specific protease 2. *Mol Cell Biol*. 2006;26(12):4675–4689.
16. Iiyama K, et al. Patterns of vascular cell adhesion molecule-1 and intercellular adhesion molecule-1 expression in rabbit and mouse atherosclerotic lesions and at sites predisposed to lesion formation. *Circ Res*. 1999;85(2):199–207.
17. Monvoisin A, Alva JA, Hofmann JJ, Zovein AC, Lane TF, Iruela-Arispe ML. VE-Cadherin-Cre-ERT2 transgenic mouse: a model for inducible recombination in the endothelium. *Dev Dyn*. 2006;235(12):3413–3422.
18. Dunn J, et al. Flow-dependent epigenetic DNA methylation regulates endothelial gene expression and atherosclerosis. *J Clin Invest*. 2014;124(7):3187–3199.
19. Nam D, et al. Partial carotid ligation is a model of acutely induced disturbed flow, leading to rapid endothelial dysfunction and atherosclerosis. *Am J Physiol Heart Circ Physiol*. 2009;297(4):H1535–H1543.
20. Merino H, Parthasarathy S, Singla DK. Partial ligation-induced carotid artery occlusion induces leukocyte recruitment and lipid accumulation — a shear stress model of atherosclerosis. *Mol Cell Biochem*. 2013;372(1):267–273.
21. Gerloff J, Korshunov VA. Immune modulation of vascular resident cells by Axl orchestrates carotid intima-media thickening. *Am J Pathol*. 2012;180(5):2134–2143.
22. Barbas CF III, Burton DR, Scott JK, Silverman GJ. *Phage Display: A Laboratory Manual*. New York, New York, USA: Cold Spring Harbor Laboratory Press; 2011.
23. Haidaris CG, et al. Recombinant human antibody single chain variable fragments reactive with Candida albicans surface antigens. *J Immunol Methods*. 2001;257(1):185–202.
24. Shea C, Bloedorn L, Sullivan MA. Rapid isolation of single-chain antibodies for structural genomics. *J Struct Funct Genomics*. 2005;6(2):171–175.
25. Takahashi M, Berk BC. Mitogen-activated protein kinase (ERK1/2) activation by shear stress and adhesion in endothelial cells. Essential role for a herbimycin-sensitive kinase. *J Clin Invest*. 1996;98(11):2623–2631.
26. Reinhart-King CA, Fujiwara K, Berk BC. Physiologic stress-mediated signaling in the endothelium. *Methods Enzymol*. 2008;443:25–44.
27. Abe J, Takahashi M, Ishida M, Lee JD, Berk BC. cASrc is required for oxidative stress-mediated activation of big mitogen-activated protein kinase 1. *J Biol Chem*. 1997;272(33):20389–20394.
28. Galluzzi L, et al. Guidelines for the use and interpretation of assays for monitoring cell death in higher eukaryotes. *Cell Death Differ*. 2009;16(8):1093–1107.
29. Ding B, et al. Left ventricular hypertrophy in ascending aortic stenosis mice: anoikis and the progression to early failure. *Circulation*. 2000;101(24):2854–2862.
30. Jiang M, Chiu SY, Hsu W. SUMO-specific protease 2 in Mdm2-mediated regulation of p53. *Cell Death Differ*. 2011;18(6):1005–1015.
31. Lessner SM, Prado HL, Waller EK, Galis ZS. Atherosclerotic lesions grow through recruitment and proliferation of circulating monocytes in a murine model. *Am J Pathol*. 2002;160(6):2145–2155.